Quantum Dephasing in Carbon Nanotubes due to Electron-Phonon Coupling

Stephan Roche,[1,2] Jie Jiang,[2] François Triozon,[1,3] and Riichiro Saito[2]

[1]*CEA/DSM/DRFMC/SPSMS/GT, 17 avenue des Martyrs, 38054 Grenoble, France*
[2]*Department of Physics, Tohoku University and CREST-JST, Sendai, 980-8578, Japan*
[3]*CEA/DRT/LETI/D2NT/LSCDP, 17 avenue des Martyrs, 38054 Grenoble, France*

(Received 16 March 2005; published 8 August 2005)

We report on the effect of electron-phonon coupling on quantum transport in carbon nanotubes. The vibrational atomic displacements as well as the electron-phonon coupling strength are introduced through a time-dependent perturbation of the π-electron Hamiltonian. The effect of dephasing on the Kubo conductance is studied for metallic and semiconducting nanotubes, and from a phenomenological law, coherence length (time) scales are found to fluctuate within the range 10 to 150 nm (0.01 to 4 ps) depending on the energy of charge carriers and phonon amplitude.

DOI: 10.1103/PhysRevLett.95.076803 PACS numbers: 73.63.Fg, 72.10.Di, 73.23.−b

Single-walled metallic carbon nanotubes (SWNT) are exceptional ballistic conductors [1,2] with a vanishingly low effect of elastic disorder (vacancies, topological defects, etc.) on backscattering, and mean free paths usually larger than several micrometers, for a Fermi level close to the charge neutrality point (CNP). This has been confirmed experimentally when measuring the conductance of small diameter metallic tubes connected to palladium electrodes [3]. The use of ballistic semiconducting nanotubes enables one to engineer preformant ballistic field effect transistors (CNT-FET) [4,5].

Ballistic transport is, however, restricted to the low bias regime, for which inelastic scattering with acoustic modes is weak [6]. Indeed, when sufficiently large bias regimes are applied to drive the electrical current, higher energy vibrational modes are activated and electron-phonon coupling limits ballistic transport. Typically, when charge carriers acquire energies above the optic phonon energies ($\simeq$180 meV), π electrons suffer inelastic scattering with optic modes, which leads to current saturation and nanotube breakdown [7]. Electron-phonon coupling in carbon nanotubes has recently been investigated in relation with temperature-dependent resistivity in metallic carbon nanotubes [8], excited-state carrier lifetime [9–11], excitonic physics [12], temperature dependence of the band gap of semiconducting nanotubes [13], or superconductivity [14].

Experimentally, Park and co-workers [15] have tentatively estimated the inelastic mean free paths (ℓ_{ie}) in both low and high bias regimes, on the basis of a phenomenological law between the measured conductance and ℓ_{ie}. In the low bias regime, their measurement indicates that $\ell_{ie} \simeq 1.6\ \mu$m and was attributed to acoustic modes (ℓ_{ac}), whereas, for bias voltage in the order of 1 V, $\ell_{ie} \simeq 10$ nm was assigned to optic (ℓ_{opt}) and/or zone-boundary phonons (ℓ_{zb}). Within the framework of effective mass formula and deformation potential approximation [6,15], the theoretical electron-acoustic phonon scattering length was estimated to be $\ell_{ac} \simeq 2.4\ \mu$m in the low bias, while $\ell_{opt} \simeq 180$ nm and $\ell_{zb} \simeq 37$ nm in the high bias regime. By applying a Mathiessen rule, the authors conclude that the total scattering length should be about 30 nm. Differently, Javey *et al.* [3] use a CNT-FET experiment, and by fitting with semiclassical Monte Carlo models, they estimate $\ell_{ac} \simeq 300$ nm and $\ell_{opt} \simeq 15$ nm for acoustic and optic modes, respectively. Thus, the reported values for inelastic mean free paths strongly fluctuate within the range [10 nm, 200 nm] for the case of electron-(optical) phonon coupling.

On the other hand, by studying the weak-localization regime in multiwalled carbon nanotubes, an energy dependence of the coherence length due to electron-electron scattering was reported [16]. The coherence length was found to be systematically smaller at the onsets of new electronic subbands. Since electron-electron and electron-phonon scattering are two different sources of quantum dephasing, the possibility of an energy dependence of the coherence length scales due to electron-phonon coupling is thus an open and challenging issue.

In this Letter, we investigate quantum dephasing and decoherence of electronic transport in carbon nanotubes, due to the coupling of electrons to the vibrational modes. Our numerical approach consists of computing the time-dependent quantum dynamics of electronic wave packets (for π electrons), under the action of a time-dependent Hamiltonian that mimics the atomic distortions in real space, as well as the strength of electron-phonon coupling. For selected phonon modes (acoustic or optical), the time-dependent Schrödinger equation (TDSE) is solved [17], and, from the Kubo conductance, the coherence length scales are extracted by using a phenomenological law [18] and assuming no contribution of elastic scattering (defects, impurities, etc.) and quantum interference effects.

The real space resolution of the TDSE is performed based on a method developed elsewhere [17]. The initial starting Hamiltonian is the π-effective model $H = \Sigma_{ij}\gamma_{ij}|\pi_i\rangle\langle\pi_j|$ with zero on-site energies and overlap integrals between $|\pi_i\rangle$ and $|\pi_j\rangle$ orbitals that are restricted to first neighbors and are given by $\gamma_{ij} = \gamma_0$ for all pairs (in the case with zero phonons). The effect of phonon vibra-

tions and electron-phonon couplings is then included by assuming that propagating wave packets will suffer from a time-dependent change of the electronic energetics (γ_{ij} matrix) of the underlying effective Hamiltonian. In a weakly disordered two-dimensional system, similar treatment of time-dependent perturbation in the weak localization regime has been shown to correctly describe frequency-dependent conductivity corrections [19].

The electron-phonon interaction is found, assuming phonon modulation of the hopping interaction: $\gamma_0 \rightarrow \gamma(r_{i,i+\delta})$, where $r_{i,i+\delta}$ is the bond length,

$$H = \sum_{i\delta} \gamma(r_{i,i+\delta})[|\pi_i\rangle\langle\pi_{i+\delta}| + \text{H.c.}], \tag{1}$$

where the bond-length-dependent Hamiltonian matrix element γ is calculated by using the analytical expression given by Porezag *et al.* [20]. The C-C bond length is $r_{i,i+\delta} = \hat{\delta} \cdot (\mathbf{R}_{i+\delta} - \mathbf{R}_i)$, with $\hat{\delta}$ the bond direction. The atomic positions for a given phonon mode with wave vector $\mathbf{q}$ and frequency $\omega_{\mathbf{q}}$ are given by

$$\mathbf{R}_i = \mathbf{R}_i^0 + A_{\mathbf{q}} \mathbf{e}_i(\mathbf{q}) \cos(\mathbf{q} \cdot \mathbf{R}_i^0 + \omega_{\mathbf{q}} t), \tag{2}$$

where $\mathbf{R}_i^0$ are the equilibrium atomic positions, while A and $\mathbf{e}$ are the phonon amplitude and eigenvector. As usual, the phonon amplitude can be expressed by [21]

$$A_{\mathbf{q}} = \sqrt{\frac{\hbar n_{\mathbf{q}}}{2M\omega_{\mathbf{q}}}}. \tag{3}$$

Here M is the carbon mass, while $n_{\mathbf{q}}$ is the phonon occupation number. For thermal equilibrium, $n_{\mathbf{q}}$ is the Bose-Einstein occupation factor, $n_{\mathbf{q}} = \frac{1}{e^{\beta\epsilon}-1}$ for phonon absorption, and $n_{\mathbf{q}} = \frac{1}{e^{\beta\epsilon}-1} + 1$ for phonon emission with $\beta = k_B T$ and ϵ phonon energy.

The phonon dispersion relations and eigenvectors are computed from the dynamical matrix in a SWNT [1]. Because of the C_N symmetry of the SWNT, the $6N \times 6N$ dynamical matrix is decoupled to N 6×6 matrices (N number of hexagons in a nanotube unit cell) [9]. We then work within the graphite unit cell, which has only one (A, B) atom pair. In the calculations, we choose the z axis along the tube axis and the x axis passing through the A atom in the unit cell.

The phonon polarization vector plays an important role in the electron-phonon coupling. Among the zone-center phonon modes, the longitudinal optic (LO) mode is the only one to contribute to inelastic backscattering, whereas among the boundary phonon modes, the dominating contribution comes from the A_1' mode [6,15]. For the LO mode, the two atoms of the unit cell move one against the other along the z axis. For the A_1' mode, the polarization vectors are given by $\mathbf{e}_A = (0, e^{-i\pi/6}, ie^{-i\pi/6})/2$ and $\mathbf{e}_B = U(\theta_{AB})(0, -i, -1)/2$ with $U(\theta_{AB})$ the rotation operator from the A to the B atom along the z axis. The electron-phonon matrix element for the A_1' mode is about $\sqrt{2}$ times that for the LO mode due to their different polarization vectors [15].

Under the hypothesis of thermalized phonon occupation at room temperature, for the LO or the A_1' mode $n_{\mathbf{q}} \approx 0$ and 1 for the phonon absorption and emission processes, respectively. The corresponding phonon amplitude for the LO mode in the case of phonon emission is labeled as A_0. However, it has recently been pointed out that this hypothesis does not hold during high-field electron transport since the high-energy phonon's excitation rate is faster than their thermalization rate and hot phonon generation can occur [22]. The phonon occupation number for the absorption process is estimated to be in the range of 2.7–5 [22].

The TDSE is solved by dividing the total evolution time ($t = n\Delta T$) in small time steps ΔT, during which the Hamiltonian energetics is kept constant. This expresses as $|\Psi(t)\rangle = \Pi_{\alpha=1,n} e^{-iH_\alpha \Delta T}|\Psi(0)\rangle$, where the whole $\gamma_{ij}(\alpha)$ coupling factors as well as on-site energies (defining H_α) will be modified according to the dynamical motion of atomic coordinates, given by Eqs. (1) and (2). The starting wave packet is a normalized random phase state that allows efficient treatment of transport in the coherent regime [17]. The γ_{ij} terms are modulated by the phonon modes, encoding the information on phonon frequency, polarization vector, and amplitude [9]. The chosen time step is about one-tenth the oscillation period of the considered phonon mode (given in units of $\hbar/\gamma_0$, so $\Delta T = 1$ corresponds to 0.227 fs). We have considered the effect of low-energy modes (acoustic and radial breathing modes) with a time period on the order of 100 fs and a longitudinal optic mode for which the period is 20 fs. The chosen time step was $\Delta T = 7(\hbar/\gamma_0) \simeq 1.6$ fs, and the total evolution time $t = 35\,000\hbar/\gamma_0 \sim 10$ ps, so that the maximum propagation length for ballistic transport is on the order of 5 μm. Our chosen (10, 10) nanotube has about 20 000 unit cells (total length of $\sim$5 μm), with periodic boundary conditions, a fact that allows one to avoid boundary effects, as explained elsewhere [17].

The quantum conductance is computed within the Kubo framework [17,18]. The spreading properties of quantum wave packets are investigated by computing the diffusion coefficients that are given by $\text{Tr}\{\delta(E - H) \times [\hat{X}(t) - \hat{X}(0)]^2\}/\text{Tr}[\delta(E - H)]$, where $\delta(E - H)$ is the spectral measure operator, whose trace gives the total density of states $n(E)$, while $\hat{X}(t)$ is the position operator in the Heisenberg representation. From the time dependence of $L^2(E, t) = \langle\Psi(0)|[\hat{X}(t) - \hat{X}(0)]^2|\Psi(0)\rangle$, one derives the scaling properties of the Kubo conductance [17]. By defining $\tau(L)$ the time at which $L^2(t) = L^2$, the conductance at such a scale is defined by $G \simeq e^2 n(E) L(\tau(L))/\tau(L)$.

In Fig. 1, we show the modifications of the electronic conductance for acoustic (LA), longitudinal optic (LO), and zone-boundary A_1' vibrational modes. The LA mode yields a vanishing (time-independent) contribution to backscattering expected at the energy ± 0.2 eV where the

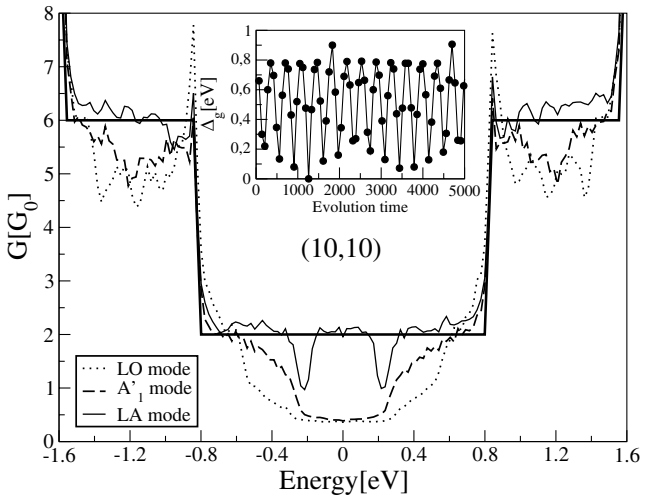

FIG. 1. Conductance for a metallic (10, 10) tube (main frame) at time $t = 35\,000\hbar/\gamma_0$ and with electron-phonon coupling, respectively, corresponding to the LO mode (dotted line), LA mode (solid line), and A_1' mode (dashed line). The bold line gives the available conduction channel in the $G_0 = 2e^2/h$ unit, and the phonon amplitude is A_0 for all curves. Inset: Time dependence of the energy gap Δ_g for distorted nanotubes encoding LO-mode displacements (time evolution is in $\hbar/\gamma_0$ unit).

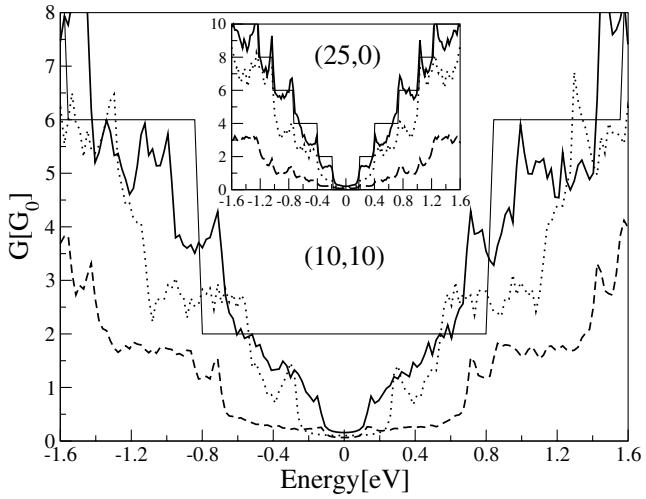

FIG. 2. Conductance for a metallic (10, 10) tube (main frame) and a semiconducting (25, 0) tube (inset) with electron-phonon coupling. The effective phonon amplitude is A_0 (solid curve), $2A_0$ (dotted curve), and $5A_0$ (dashed curve). The solid lines give the exact number of quantum channels $N_\perp$.

observation of a stepwise reduction of the conductance is attributed to a phonon-induced symmetry breaking effect. In contrast, high-energy modes produce a much larger reduction of $G(E)$ in the central region around the CNP, as well as for higher energies. Besides, the scaling properties of conductance patterns are found to fluctuate owing to time-dependent band structure changes. Indeed, a comparison between equilibrium band structure and the electronic spectrum of a distorted nanotube, encoding the atomic displacements of high-energy modes, demonstrates the occurrence of shifts of the electronic bands that scale linearly with the distortion amplitude [10]. This complex dynamical phenomenon is here illustrated in the time evolution of an energy gap Δ_g of the density of states of the (10, 10) nanotube, which fluctuates periodically in time following the symmetry changes of the LO-mode driven distorted nanotube atomic configurations (Fig. 1, inset).

We now focus on the impact of LO phonon modes, as the main inelastic source of dephasing and decoherence. By considering the hot phonon occupation and the enhanced electron-phonon coupling by the A_1' phonon, we let the amplitude vary within $[A_0, 5A_0]$. The conductance as a function of Fermi energy and amplitude of the electron-phonon coupling are shown for a typical (10, 10) metallic nanotube (Fig. 2, main frame) and a (25, 0) semiconducting nanotube (Fig. 2, inset). The increase of the phonon amplitude progressively degrades the conductance all over the spectrum, although some fluctuations are seen in the surrounding of the Van Hove singularities. Close to the onsets of new subbands (defined by the energies of the Van Hove singularities), the conductance remains larger in regards to the rest of the spectrum. This originates from the reduced velocity of charge carriers at those energies, which results in lower propagating length $L(E, t) = v(E)t$ (for the same evolution time t), and a weaker contribution of electron-phonon coupling. Note that different phonon amplitudes also result in some band structure changes, which are reflected in a few energies where the conductance of the A_0 case becomes smaller than the $2A_0$ case [seen only for the (10, 10) tube].

Now to extract the coherence length scales, we proceed as follows. In the pure ballistic case, the conductance is given by $G(E) = N_\perp(E)G_0$, with $N_\perp(E)$ the number of conducting channels at a given energy E, and $G_0 = 2e^2/h$ the conductance quantum. Whenever decoherence will take place, the Kubo conductance will downscale, and in a first approximation [15,18]

$$G(E, t) = \frac{2e^2}{h}\frac{N_\perp(E)L_\phi(E)}{L(E, t)}, \tag{4}$$

where $L(E, t)$ is the length scale that is energy dependent due to velocity $v(E)$ and scales linearly with time. As long as the propagating length $L(E, t)$ remains lower than the real coherence length, the conductance keeps its ballistic value, and applying Eq. (4) gives thus a quantity $2e^2N_\perp(E)/h$ that is time independent. When $G(E, t)$ starts to decrease in time, then $L_\phi(E)$ extracted from Eq. (4) becomes smaller than $L(E)$. This transition allows one to estimate the physical coherence length. At a fixed phonon amplitude (A_0) of the LO mode, $L_\phi(E)$ was studied for several armchair nanotubes {(5, 5), (10, 10), (15, 15)}. The results (not shown here) show that the coherence length amplitude is strongly modulated at the onsets of new subbands, whose positions vary from one nanotube to another.

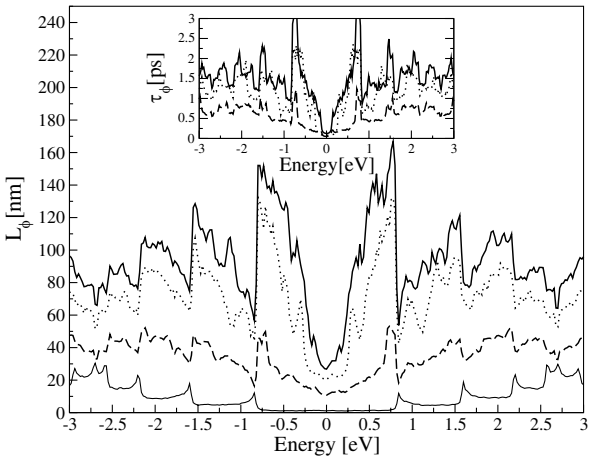

FIG. 3. Main frame: $L_\phi(E)$ for the (10, 10) armchair nanotube in the presence of the LO mode, evaluated at $t = 7000\hbar/\gamma_0$, for several phonon amplitudes corresponding to A_0 (solid line), $2A_0$ (dotted line), and $5A_0$ (dashed line). Inset: Corresponding coherence times evaluated from $\tau_\phi(E) = L_\phi(E)/v(E)$ for the same parameters. The rescaled density of states is also shown in the main frame (thin solid line).

The effect of phonon amplitude on $L_\phi(E)$ for the (10, 10) nanotube is shown in Fig. 3. The fluctuations of $L_\phi(E)$ are driven by the onsets of new subbands. We first observe that in all cases, $L_\phi(E)$ becomes smaller at the position of Van Hove singularities, which is similar to the experimental results reported for the electron-electron scattering situation [16]. By increasing the effective amplitude from A_0 to $5A_0$, the coherence length is gradually reduced, and the fluctuations are smoothened. For the stronger modulation amplitude, $L_\phi(E)$ is found to fluctuate within the range [10 nm, 150 nm] for the considered energy window. One notes that such a range of values corresponds to the prior estimates for electron-phonon scattering lengths [3,15], but in our case their absolute values are fixed by the chosen evolution time, so that only relative fluctuations are physically relevant. By using $\tau_\phi = L_\phi(E)/v(E)$, one deduces the corresponding coherence times (Fig. 3, inset), which range within [0.01 ps, 0.4 ps], depending on phonon amplitude and energy of charge carriers. Spectroscopic experiments allow one to estimate some typical values for electron-(optic) phonon scattering times on the order of 0.1–0.4 ps [9,10], so in good agreement with the present coherence time scales, validating our choice for the fixed evolution time ($t = 35000\hbar/\gamma_0$).

In conclusion, the effect of electron-(optical) phonon coupling was found to strongly affect electronic conductance and to induce some energy dependence of the coherence length scale, similar to the experimental data obtained in the weak-localization regime [16]. All the calculations have, however, been done at room temperature, assuming clean nanotubes. Further works should put more emphasis on temperature effects, to more quantitatively address the challenging issues of nanotube-based field effect transistor performances or the temperature dependence of the coherence length scale in the weak localization regime.

S. R. acknowledges support from ACI grant Transnanofils and the CREST/JST for supporting his work in Japan. R. S. acknowledges a Grant-in-Aid (No. 16076201) from the Ministry of Education, Japan. S. R. is indebted to Xavier Blase for his encouragements and suggestions.

[1] R. Saito, G. Dresselhaus, and M. S. Dresselhaus, *Physical Properties of Carbon Nanotubes* (Imperial College Press, London, 1998).
[2] C. T. White and T. N. Todorov, Nature (London) **393**, 240 (1998); Paul L. McEuen *et al.*, Phys. Rev. Lett. **83**, 5098 (1999).
[3] A. Javey *et al.*, Phys. Rev. Lett. **92**, 106804 (2004).
[4] Ph. Avouris, MRS Bull. **29**, 403 (2004).
[5] A. Javey *et al.*, Nature (London) **424**, 654 (2003).
[6] H. Suzuura and T. Ando, Phys. Rev. B **65**, 235412 (2002); L. M. Woods and G. D. Mahan, Phys. Rev. B **61**, 10 651 (2000); G. Pennington and N. Goldsman, Phys. Rev. B **68**, 045426 (2003).
[7] P. G. Collins *et al.*, Phys. Rev. Lett. **86**, 3128 (2001).
[8] C. L. Kane *et al.*, Europhys. Lett. **41**, 683 (1998).
[9] J. Jiang *et al.*, Phys. Rev. B **71**, 045417 (2005).
[10] S. Reich *et al.*, Phys. Rev. B **71**, 033402 (2005); M. Máchon *et al.*, Phys. Rev. B **71**, 035416 (2005).
[11] V. Perebeinos, J. Tersoff, and Ph. Avouris, Phys. Rev. Lett. **94**, 086802 (2005).
[12] V. Perebeinos, J. Tersoff, and Ph. Avouris, Phys. Rev. Lett. **94**, 027402 (2005).
[13] R. B. Capaz *et al.*, Phys. Rev. Lett. **94**, 036801 (2005).
[14] X. Blase, Ch. Adessi, and D. Connétable, Phys. Rev. Lett. **93**, 237004 (2004).
[15] Ji-Yong Park *et al.*, Nano Lett. **4**, 517 (2004).
[16] B. Stojetz *et al.*, Phys. Rev. Lett. **94**, 186802 (2005).
[17] F. Triozon *et al.*, Phys. Rev. B **69**, 121410 (2004); S. Roche, Phys. Rev. B **59**, 2284 (1999); S. Latil *et al.*, Phys. Rev. Lett. **92**, 256805 (2004).
[18] E. Akkermans and G. Montambaux, *Physique Mésoscopique des Électrons et des Photons* (EDP Sciences, Paris, 2004).
[19] H. Watanabe *et al.*, J. Phys. Soc. Jpn. **72**, 645 (2003).
[20] D. Porezag, Th. Frauenheim, and Th. Köhler, Phys. Rev. B **51**, 12 947 (1995).
[21] P. K. Lam, M. M. Dacorogna, and M. L. Cohen, Phys. Rev. B **34**, 5065 (1986).
[22] M. Lazzeri *et al.*, cond-mat/0503278.